Three-Dimensional Maneuver Control of Multiagent Systems With Constrained Input

Yu-Wen Chen, Ming-Li Chiang, *Member, IEEE*, and Li-Chen Fu, *Fellow, IEEE*

***Abstract*—In this article, we propose a new 3-D maneuver controller for a class of nonlinear multiagent systems (MASs) with nonholonomic constraint and saturated control. The system is designed under a distributed communication topology and the controller is more flexible and efficient for general formation maneuver tasks. The saturation design generates control inputs within pregiven bounds, which makes the system more applicable in practice. Moreover, based on the nonholonomic model, the proposed control also considers the heading angles of the agents. Thus, the maneuver controller can achieve a more natural tracking movement where the heading of the formation will align to the direction of the reference trajectory during the tracking motion. Several simulation examples are given to validate our results and demonstrate the competence for various maneuver tasks of MASs.**

***Index Terms*—Distributed control, input saturation, multiagent system (MAS), nonlinear systems.**

I. Introduction

RECENTLY, control of multiagent system (MAS), especially with the quadrotor agents, has drawn significant attention and many research results are developed due to its extensive applications. With the lower cost and the rapid developments of robotics and microunmanned aerial vehicles (MUAVs), the research field grows prosperously. Maneuver control, which aims to steer the agents to form into a desired geometric pattern and perform specified motions, is one of the important topics in the research of MAS. Various maneuver control may include tracking a given trajectory [1]–[6], rotating [6]–[8], or scaling the formation [1], [3], [6], etc. In this article, we design a new distributed nonlinear maneuver controller in 3-D space for the MAS with input saturation, which can achieve general maneuver tasks. For existing results of formation and maneuver control of MAS, we discuss it from three aspects as follows, which are the model of agents, the characteristics of formation control strategies, and the communication links in MAS. As for the model of agents, most of the studies model them by a single integer [9], double integrator [10], [11], or a linear system [3], [8], [12], [13], where many interesting results are proposed. On the other hand, in practical applications, many actual agents, such as robots and UAVs, are not suitable to be modeled by a linear model. Therefore, works that consider the nonlinear model for the agents arise. For example, [14]–[16] represent the agents by unicycle models where the nonholonomic constraint is considered. For such nonlinear model, the heading angle can be addressed and even lead to applications that utilizes the formation direction. For the characterizations of formation strategies, the formation control can be classified by the sensing ability and control variables. In [17], the types of formation controller are categorized into the position-based control [18], distance-based control [19], and displacement-based control. Recently, the bearing-based approach has attracted much attention based on the transformable control [1], [16], [20], [21]. The third aspect is the communication links between agents. Generally speaking, the signal strength fades away rapidly with communication range, which restricts the construction of available links. As the computation loads raise with the number of communication links, more research progress from global communications to local one [8], [13], [22], [23], from centralized to decentralized [8], [10], [24]–[26], and from static to switching [27]. To release the global communications, estimation of the reference signals is required. There are some new adaptive estimation method developed for nonlinear systems, such as [28] and [29], where the adaptive fuzzy and adaptive neural network control are designed. In this article, we propose the consensus process and adaptive estimations to support the distributed communication scenario.

To implement the maneuver controller, there are also many researches considering the physical constraints of the MAS, such as input saturation. Control with saturated input is an important issue for practical applications and there are many existing results related to this problem, especially for the linear systems. As discussed in [30], stabilization of systems with saturation can be classified into two main approaches. One is the positively invariant approach, which makes the controller always work inside the saturation region, and another

Manuscript received 30 September 2020; revised 24 September 2021 and 15 January 2022; accepted 28 March 2022. Date of publication 25 April 2022; date of current version 16 September 2023. This work was supported by the Ministry of Science and Technology of Taiwan and Center for Artificial Intelligence and Advanced Robotics, National Taiwan University under Grant MOST 110-2221-E-002-166-MY3, Grant MOST 110-2634-F-002-049, Grant MOST 110-2221-E-029-028, and Grant MOST 109-2221-E-029-026. This article was recommended by Associate Editor Y.-J. Liu. *(Corresponding author: Ming-Li Chiang.)*

Yu-Wen Chen is with the Department of Electrical Engineering and Computer Science, University of California at Berkeley, Berkeley, CA 94720 USA (e-mail: yuwen_chen@berkeley.edu).

Ming-Li Chiang is with the Department of Applied Mathematics, Tunghai University, Taichung 407224, Taiwan (e-mail: mingli@ntu.edu.tw).

Li-Chen Fu is with the Department of Electrical Engineering, the Department of Computer Science and Information Engineering, and the Center of Artificial Intelligence and Advanced Robotics, National Taiwan University, Taipei 112, Taiwan (e-mail: lichen@ntu.edu.tw).

Color versions of one or more figures in this article are available at https://doi.org/10.1109/TCYB.2022.3165767.

Digital Object Identifier 10.1109/TCYB.2022.3165767

approach permits the control to reach saturation while attaining the stability. Lian and Wu [30] considered the invariant set approach and design the stabilizing controller with the semiellipsoids. In our article, we design the saturated control by transforming the original model such that the linear velocity and angular velocity are decoupled, and thus, the saturation bound can be reached to meet the control target. In [5], [11], [26], and [31]–[34], formation controllers with constrained input are discussed for linear models. However, there are relatively few works consider constrained input with nonlinear models such as [4], where only planar motion is discussed. In this article, we propose a new 3-D nonlinear maneuver controller with input saturation and nonholonomic constraint, while being able to achieve various maneuver tasks. Among those tasks, we especially address the design for a more natural tracking movement, where we control the heading of the formation to align to the moving direction of the reference trajectory. Moreover, for another physical constraint—nonholonomic constraint, in [3], [20], [21], and [35]–[37], 3-D motions or higher order models of MAS are considered; however, these results are obtained with the linear model, which do not cover the issue. While in [2], [15], [16], and [38], they consider nonholonomic agents; however, only 2-D system or inputs without saturation are discussed. In this article, we consider design in the 3-D space and deal with nonholonomic and saturation constraints to proceed the implementation of controller in reality.

In summary, the main contributions of this article are listed as follows.

1) We propose a novel 3-D nonlinear maneuver controller for MAS, which covers most maneuver tasks proposed in existing results, for example, tracking, rotating, and transforming. In addition, due to the capability of 3-D tracking and the proposed two-phase scheme that contains cooperative design and local tracking, we can achieve the hierarchical structure maneuver, which provides much more flexibility and efficiency.
2) The proposed design addresses the issue of directions of agent headings. By decoupling the goal of formation heading into the preknown and online decision part, our design allows the MAS to track in arbitrary formation orientation. Most existing tracking results, [9], [23], [32], [33], to name a few, require prespecified displacements from formation centroid to desired positions, which leads to fix orientation when tracking. In contrast, our design retrieves additional information in formation progress, which motivating a more natural tracking movements that cannot be extended from existing works.
3) We design a novel nonlinear controller with saturation where the design introduces a two-phase scheme that contains a global and a local design, as in the navigation problem. More precisely, a globally planned guidance trajectory is first cooperatively determined, and then agents will decide local trajectory with the consideration of saturation based on the planned guidance trajectory.

The remainder parts of this article are organized as follows. In Section II, we give a brief introduction of graph theory and our control targets. In Section III, a novel description of the desired formation pattern and problem formulation is given. Section IV shows the main design result and Section V proposes the saturated control. In Section VI, we provide some extensions of the proposed design, including the pattern-varying formation and switching communications. Section VII provides four simulation examples and the conclusion is given in Section VIII.

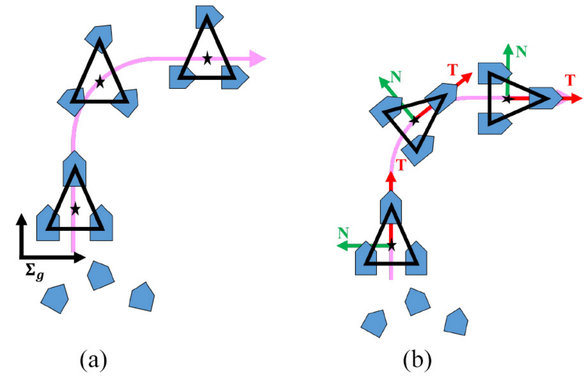

Fig. 1. Planar maneuver control of MAS with and without heading alignment. (a) Fixed formation orientation case. (b) Natural tracking case.

II. Preliminaries

In this section, we provide some terms in graph theory to represent the communication links in the MAS. In addition, we introduce the concept of "natural tracking," which is a novel function that we endow with the MAS.

A. Algebraic Graph Theory

A N-node directed graph $\mathcal{G} = (V, E)$ is composed of N nodes $V = \{V_1, \dots, V_N\}$ and a set of directed edges E. An edge pointing from $V_j \in V$ toward $V_i \in V$ is denoted as $(i, j) \in E$. In MAS, graph is a tool often used to describe the communication links, where V_i represents the agents-i and an edge $(i, j) \in E$ implies that agent-i can receive information from agent-j. For agent-i, the collection of all accessible agents is denoted as N_i, that is, $N_i = \{V_j | (i, j) \in E\}$, which are called neighbors. $|N_i|$ is the number of agent-i's neighbors. Some related matrices are defined as follows. The adjacency matrix $\boldsymbol{A} = [a_{ij}] \in \mathbb{R}^{N\times N}$ is defined where $a_{ij} = 1$ if $(i, j) \in E$, and 0 otherwise. The in-degree matrix $\boldsymbol{D} = [d_{ii}] \in \mathbb{R}^{N\times N}$ is a diagonal matrix with $d_{ii} = |N_i|$. The Laplacian matrix $\boldsymbol{L} \in \mathbb{R}^{N\times N}$ is defined as $\boldsymbol{D} - \boldsymbol{A}$.

B. Maneuver Control With "Natural Tracking"

Before explaining the concepts of "natural tracking" of a MAS, we first turn to the single agent case. In a single robot tracking case, steering its heading to align with moving direction is a common job as a human looks ahead when walking. We call the moving scenario as "natural tracking." To generalize this idea to MASs, we say that a MAS tracks "naturally" if the heading of the formed geometric pattern keeps tangent to the tracking trajectory. An illustration of fixed-orientation tracking versus natural tracking is provided in Fig. 1. In natural tracking case, Fig. 1(b), not only headings of individuals spin when tracking trajectory turns but also the heading of the geometric pattern rotates. As a comparison, only individuals' headings rotate in fixed-orientation case [Fig. 1(a)]. The natural tracking case is a more expected movement in daily applications such as formation flying. Unfortunately, most of the existing results, such as [15], [16], and [22], to name a few, focus on fixed-orientation tracking, and moreover, these design cannot directly extend to natural tracking case, which will be discussed in Section II-C. As a result, we will provide a novel design to endow MASs with the ability of natural tracking in Section III.

C. Simplified Problem and Existing Controller Design

Briefly speaking, we aim to design a controller such that the MAS can achieve natural tracking while maintaining the desired geometric pattern in the 3-D space. In this section, we will first demonstrate a simplified problem for controller design. Then, some insufficiency will be pointed out subsequently, which motivates the complete problem and the design concept in Section III.

Consider an N-agent MAS with subindex set $\mathcal{N} = \{1, \ldots, N\}$. The 3-D dynamics are given as

$$\dot{\boldsymbol{x}}_i = \boldsymbol{A}\boldsymbol{x}_i + \boldsymbol{B}u_i \tag{1}$$

for $i \in \mathcal{N}$, where $\boldsymbol{x}_i \in \mathbb{R}^3$ and $u_i \in \mathbb{R}$ are agent-i's position and scalar control input, respectively. $\boldsymbol{A} \in \mathbb{R}^{3\times 3}$ and $\boldsymbol{B} \in \mathbb{R}^{3\times 1}$ are constant matrices. Given a tracking reference $\boldsymbol{r}_0(t) \in \mathbb{R}^3$ where the centroid of the MAS should follow, and a formation configuration that describes the desired geometric pattern, $\boldsymbol{h} = [\boldsymbol{h}_1^T, \ldots, \boldsymbol{h}_N^T]^T \in \mathbb{R}^{3N}$, where $\boldsymbol{h}_i \in \mathbb{R}^3$ indicates the desired displacement of agent-i from the centroid in desired geometric pattern. Then, based on a given communication graph $\mathcal{G}$, the objective is to design u_i such that the MAS achieves tracking and formation, that is, $\boldsymbol{x}_i \to \boldsymbol{r}_0 + \boldsymbol{h}_i \ \forall i \in \mathcal{N}$.

However, since $\boldsymbol{h}$ is a constant vector, when the goal is succeeded, the MAS is actually tracking with a fixed orientation, as in [9], [23], [32], and [33], to name a few, depicted by Fig. 1(a). In order to achieve natural tracking, as in Fig. 1(b), the constant $\boldsymbol{h}$ requires modification by multiplying a varying rotation signal $\boldsymbol{R_h}(t) \in SO(3)$. The modified signal $\boldsymbol{R_h}(t)$ is determined by rotating the corresponding angle such that the heading of the pattern is aligned to the moving direction at time t. Namely, a modified time-varying configuration $\boldsymbol{h}_m(t) := (\boldsymbol{R_h}(t) \otimes \boldsymbol{I}_N)\boldsymbol{h} = [\boldsymbol{h}_{m1}^T(t), \ldots, \boldsymbol{h}_{mN}^T(t)]^T \in \mathbb{R}^{3N}$ is now considered, where $\otimes$ denotes the Kronecker product. Correspondingly, we now aim to design control input u_i such that $\boldsymbol{x}_i \to \boldsymbol{r}_0 + \boldsymbol{h}_{mi} \ \forall i \in \mathcal{N}$. The problem becomes MAS time-varying formation control with linear dynamics. As a result, one may refer to the results of time-varying formation as in [8] and [27] and propose design as

$$\begin{aligned} u_i = {}& \boldsymbol{K}_1\boldsymbol{x}_i + \boldsymbol{K}_2(\boldsymbol{x}_i - \boldsymbol{h}_{mi}) + \alpha\boldsymbol{K}_3 \sum_{j\in N_i}\left(x_j - \boldsymbol{h}_{mj}\right) \\ & - \ (\boldsymbol{x}_i - \boldsymbol{h}_{mi}) + v_i \end{aligned} \tag{2}$$

for $i \in \mathcal{N}$, where $\boldsymbol{K}_1, \boldsymbol{K}_2, \boldsymbol{K}_3 \in \mathbb{R}^{1\times 3}$ are constant matrices, α is weighting parameter, and $v_i \in \mathbb{R}$ is a time-varying signal associated with $\boldsymbol{h}_{mi}(t)$.

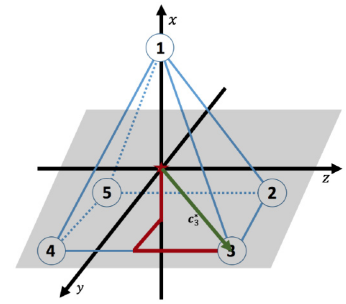

Fig. 2. Descriptions.

It seems that the natural tracking problem can be solved by (2), in fact, the solution is infeasible. In the following, we will explain the infeasibility and point out some details overlooked in this simplified problem. Then, the complete problem and the novel design are proposed in Section III.

The infeasibility originates from the modified signal $\boldsymbol{R_h}(t)$. The determination of $\boldsymbol{R_h}(t)$ is based on the assumptions that $\boldsymbol{r}_0$ is not only preknown but also globally accessible. As a result, the communication constraints are violated. Moreover, since $\boldsymbol{R_h}(t)$ is prefixed, $\boldsymbol{r}_0$ is not allowed to be online adjusted, which decreases the flexibility in real applications. In addition to the above issue, to achieve natural tracking, headings are crucial information but omitted in linear model (1), which motivates us to turn to 3-D unicycle model in the following revised problem. Overall, time-varying configuration $\boldsymbol{h}_m(t)$ for describing geometric pattern in natural tracking remains some issues. As a result, we will propose "relative description" of desired geometric pattern in the following, which facilitates the achievement of natural tracking without above concerns.

III. Relative Description of Desired Geometric Pattern and Problem Formulation

In this section, we first propose an idea to describe desired geometric pattern. Then, formulate the revised problem based on the relative description.

A. Relative Description of Desired Geometric Pattern

Given any N-vertex desired geometric pattern, say Fig. 2, there exists a centroid and a user-defined heading. Impose a coordinate whose origin is at the centroid and x-axis is aligned with the heading, as shown in Fig. 2, where the desired formation is a quadrangular pyramid pointing upward. Then, denote the vectors from the centroid to each agent as the center vectors $\boldsymbol{c}_i^* \in \mathbb{R}^3 \ \forall i \in \mathcal{N}$, which can be interpreted in sphere coordinate as $\{d_i^*, \phi_i^*, \theta_i^*\}$ with relations $\boldsymbol{c}_i^* = d_i^*[\cos\phi_i^* \cos\theta_i^*, \sin\phi_i^* \cos\theta_i^*, \sin\theta_i^*]^T$. The description is representative and determined relatively within the agents. Since the relative description is frame invariant, which implies that the description remains the same under rotation, the relative description is more suitable for natural tracking than the inaccessible time-varying signal $\boldsymbol{h}_m(t)$.

Based on the discussions in Section II-C and the proposed relative description, a revised problem is then rendered.

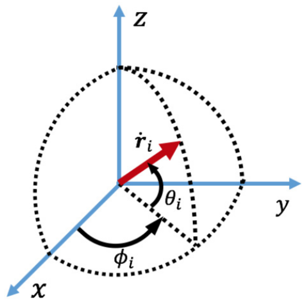

Fig. 3. Model.

B. Complete Problem Formulation

Consider an N-agent MAS with subindex set $\mathcal{N} = \{1, \ldots, N\}$. The 3-D dynamics are given as

$$\begin{aligned}\dot{\boldsymbol{r}}_i &= v_i[\cos\phi_i \cos\theta_i, \sin\phi_i \cos\theta_i, \sin\theta_i]^T \\ \dot{\phi}_i &= \omega_i, \\ \dot{\theta}_i &= u_i\end{aligned} \tag{3}$$

for $i \in \mathcal{N}$, where $\boldsymbol{r}_i \in \mathbb{R}^3$ is agent-i's position, $\phi_i \in (-\pi, \pi]$ and $\theta_i \in (-(\pi/2), (\pi/2)]$ depict agent-i's heading, as shown in Fig. 3. v_i, ω_i, and u_i are scalar control inputs.

Given a desired geometric pattern described by relative description $\{d_i^*, \phi_i^*, \theta_i^*\}$ $\forall i \in \mathcal{N}$, a communication graph $\mathcal{G}$, and a reference centroid tracking trajectory $\boldsymbol{r}_0$, which satisfies $\dot{\boldsymbol{r}}_0 = v_0[\cos\phi_0 \cos\theta_0, \sin\phi_0 \cos\theta_0, \sin\theta_0]^T, \dot{\phi}_0 = \omega_0, \dot{\theta}_0 = u_0$. Then, the goal is to design v_i, ω_i, u_i $\forall i \in \mathcal{N}$, such that the MAS can achieve natural tracking. Mathematically speaking, the objective is to propose control laws v_i, ω_i, u_i such that

$$\boldsymbol{r}_i \to \boldsymbol{r}_0 + \boldsymbol{R}_Z(\phi_0)\boldsymbol{R}_Y(-\theta_0)\boldsymbol{c}_i^* \tag{4}$$

for $i \in \mathcal{N}$, where $\boldsymbol{R}_Z$ and $\boldsymbol{R}_Y$ are rotation matrices given as

$$\boldsymbol{R}_Z(\psi) = \begin{bmatrix}\cos\psi & -\sin\psi & 0 \\ \sin\psi & \cos\psi & 0 \\ 0 & 0 & 1\end{bmatrix}, \boldsymbol{R}_Y(\psi) = \begin{bmatrix}\cos\psi & 0 & \sin\psi \\ 0 & 1 & 0 \\ -\sin\psi & 0 & \cos\psi\end{bmatrix}.$$

Note that $\boldsymbol{c}_i^*$ is with respect to relative description frame, as introduced in Section III-A. When performing natural tracking, the x-axis of relative description frame is supposed to align with direction of $\dot{\boldsymbol{r}}_0$. As a result, the second term of the right-hand side in (4) is transforming $\boldsymbol{c}_i^*$ from relative description frame to global frame. In the following, for consistency, the reference $\boldsymbol{r}_0$ will be referred as agent-0 and communication graph $\bar{\mathcal{G}}$ is extended with agent-0. Also, extend N_i in $\bar{\mathcal{G}}$ as the extended neighbor set $\bar{N}_i$ and define extended Laplacian $\bar{\boldsymbol{L}} := \boldsymbol{L} + \boldsymbol{B} \in \mathbb{R}^{N\times N}$ where $\boldsymbol{B}$ is diagonal with $b_{ii} = 1$ if agent-i communicates with agent-0.

IV. Controller Design

In this section, a crude controller design is proposed, which utilizes model transformation. The technique is similar to [39] where they construct the transformation between linear model and unicycle model. Here, we extend it to 3-D case. Through differentiation and calculations from (3), we have

$$\begin{aligned}v_i &= |\dot{\boldsymbol{r}}_i| \\ \omega_i &= \frac{[-\sin\phi_i, \cos\phi_i, 0]^T \ddot{\boldsymbol{r}}_i}{v_i \cos\theta_i} \\ u_i &= \frac{[-\cos\phi_i \sin\theta_i, -\sin\phi_i \sin\theta_i, \cos\theta_i]^T \ddot{\boldsymbol{r}}_i}{v_i}\end{aligned} \tag{5}$$

for $i \in \mathcal{N}$. Hence, we may first design $\ddot{\boldsymbol{r}}_i$ to achieve (4), then derive control inputs v_i, ω_i, and u_i via (5).

To proceed the design, we first define the position error

$$\boldsymbol{e}_i := \boldsymbol{r}_0 + \boldsymbol{R}_Z(\phi_0)\boldsymbol{R}_Y(-\theta_0)\boldsymbol{c}_i^* - \boldsymbol{r}_i \tag{6}$$

for $i \in \mathcal{N}$. Now, we try to design $\ddot{\boldsymbol{r}}_i$ such that $\boldsymbol{e}_i$ converges to $\boldsymbol{0}$. Note that v_0, ϕ_0, and θ_0, are not globally accessible due to $\bar{\mathcal{G}}$. To overcome this issue, we will apply well-known time-varying consensus algorithm, as in [40], for agents to consensus their estimations of v_0, ϕ_0, and θ_0. Similarly, an observer is proposed for agent-i to estimate $\boldsymbol{e}_i$ to overcome the nonglobally accessible issue.

A. Consensus Algorithms for v_0, ϕ_0, and θ_0

To deal with the communication issues, denote $\hat{v}_i$, $\hat{\phi}_i$, and $\hat{\theta}_i$ as the estimation of v_0, ϕ_0, and θ_0 by agent-i, respectively. Since all agent dedicate to catch up with the same signals, this is classical time-varying state consensus problem, which allows us to apply existing results, for example, [18] and [40].

Lemma 1 [40]: Suppose $\mathcal{G}$ is strongly connected and agent-0 has at least one neighbor in $\bar{\mathcal{G}}$, then the control laws

$$\ddot{\hat{v}}_i = \frac{1}{|\bar{N}_i|}\sum_{j\in\bar{N}_i}\left[\ddot{\hat{v}}_j + k_1\left(\dot{\hat{v}}_j - \dot{\hat{v}}_i\right) + k_2\left(\hat{v}_j - \hat{v}_i\right)\right] \tag{7}$$

$$\ddot{\hat{\phi}}_i = \frac{1}{|\bar{N}_i|}\sum_{j\in\bar{N}_i}\left[\ddot{\hat{\phi}}_j + k_3\left(\dot{\hat{\phi}}_j - \dot{\hat{\phi}}_i\right) + k_4\left(\hat{\phi}_j - \hat{\phi}_i\right)\right] \tag{8}$$

$$\ddot{\hat{\theta}}_i = \frac{1}{|\bar{N}_i|}\sum_{j\in\bar{N}_i}\left[\ddot{\hat{\theta}}_j + k_5\left(\dot{\hat{\theta}}_j - \dot{\hat{\theta}}_i\right) + k_6\left(\hat{\theta}_j - \hat{\theta}_i\right)\right] \tag{9}$$

will drive $\hat{v}_i \to v_0$, $\hat{\phi}_i \to \phi_0$, and $\hat{\theta}_i \to \theta_0$ exponentially, for $i \in \mathcal{N}$, where $k_i > 0$, $i = 1, \ldots, 6$, are arbitrary constants.

Proof: Refer to [40]. ■

B. Observer Design for $\boldsymbol{e}_i$

Since $\boldsymbol{e}_i$ is not globally accessible due to $\bar{\mathcal{G}}$, we denote $\hat{\boldsymbol{e}}_i$ as the estimation of $\boldsymbol{e}_i$, for $i \in \mathcal{N}$. To obtain $\hat{\boldsymbol{e}}_i$, the estimated $\boldsymbol{r}_0$, ϕ_0, and θ_0, are required. Fortunately, with consensus algorithms in Lemma 1, we have the estimation of ϕ_0 and θ_0. As a result, we define $\hat{\boldsymbol{c}}_i$ as the estimations of $\boldsymbol{R}_Z(\phi_0)\boldsymbol{R}_Y(-\theta_0)\boldsymbol{c}_i^*$ by

$$\hat{\boldsymbol{c}}_i = \boldsymbol{R}_Z\left(\hat{\phi}_i\right)\boldsymbol{R}_Y\left(-\hat{\theta}_i\right)\boldsymbol{c}_i^* \tag{10}$$

for $i \in \mathcal{N}$, where $\boldsymbol{c}_i^*$ is the relative description introduced in Section III-A. Then, $\hat{\boldsymbol{c}}_i$ satisfies the following lemma.

Lemma 2: With Lemma 1, for $i \in \mathcal{N}$, $\hat{\boldsymbol{c}}_i$ converges to $\boldsymbol{R}_Z(\phi_0)\boldsymbol{R}_Y(-\theta_0)\boldsymbol{c}_i^*$ exponentially.

Proof: We have

$$\begin{aligned}&\left\|\boldsymbol{R}_Z\left(\hat{\phi}_i\right)\boldsymbol{R}_Y\left(-\hat{\theta}_i\right)\boldsymbol{c}_i^* - \boldsymbol{R}_Z(\phi_0)\boldsymbol{R}_Y(-\theta_0)\boldsymbol{c}_i^*\right\| \\ &= \left\|\left(\boldsymbol{R}_Z\left(\hat{\phi}_i\right) - \boldsymbol{R}_Z(\phi_0)\right)\boldsymbol{R}_Y\left(-\hat{\theta}_i\right)\boldsymbol{c}_i^* \right.\\ &\quad \left. + \boldsymbol{R}_Z(\phi_0)\left(\boldsymbol{R}_Y\left(-\hat{\theta}_i\right) - \boldsymbol{R}_Y(-\theta_0)\right)\boldsymbol{c}_i^*\right\| \\ &\leq d_i^*\left\|\boldsymbol{R}_Z\left(\hat{\phi}_i\right) - \boldsymbol{R}_Z(\phi_0)\right\| + d_i^*\left\|\boldsymbol{R}_Y\left(-\hat{\theta}_i\right) - \boldsymbol{R}_Y(-\theta_0)\right\| \\ &\leq d_i^* l_1\left\|\hat{\phi}_i - \phi_0\right\| + d_i^* l_2\left\|\hat{\theta}_i - \theta_0\right\|\end{aligned}$$

where l_1 and l_2 in the last inequality are the Lipschitz constants of $\boldsymbol{R}_Z(\cdot)$ and $\boldsymbol{R}_Y(\cdot)$, respectively. Then, by the exponential convergence of $\hat{\phi}_i$ and $\hat{\theta}_i$ from Lemma 1, the exponetial convergence of $\hat{\boldsymbol{c}}_i$ is derived. ■

To derive estimated $\boldsymbol{r}_0$, note that we have actually obtained the estimation of $\dot{\boldsymbol{r}}_0$, that is, $\hat{v}_i[\cos\hat{\phi}_i\cos\hat{\theta}_i, \sin\hat{\phi}_i\cos\hat{\theta}_i, \sin\hat{\theta}_i]^T$. Therefore, an observer is competent for the task.

In the following, with Lemmas 1 and 2, we are ready to design the observer for $\hat{\boldsymbol{e}}_i$. Denote $\boldsymbol{u}(\phi,\theta)$ as the spherical unit vector $[\cos\phi\cos\theta, \sin\phi\cos\theta, \sin\theta]^T \in \mathbb{R}^3$.

Lemma 3: Suppose $\mathcal{G}$ is strongly connected and agent-0 has at least one neighbor in $\bar{\mathcal{G}}$, then the update law

$$\begin{aligned}\dot{\hat{\boldsymbol{e}}}_i &= \hat{v}_i\left[\cos\hat{\phi}_i\cos\hat{\theta}_i, \sin\hat{\phi}_i\cos\hat{\theta}_i, \sin\hat{\theta}_i\right]^T - \dot{\boldsymbol{r}}_i + \dot{\hat{\boldsymbol{c}}}_i \\ &\quad + k_7\sum_{j\in\bar{N}_i}[\hat{\boldsymbol{e}}_j - \hat{\boldsymbol{e}}_i + \boldsymbol{r}_j - \boldsymbol{r}_i + \hat{\boldsymbol{c}}_i - \hat{\boldsymbol{c}}_j]\end{aligned} \tag{11}$$

will drive $\hat{\boldsymbol{e}}_i \to \boldsymbol{e}_i$ exponentially, for $i \in \mathcal{N}$, where $k_7 > 0$ is arbitrarily chosen constant.

Proof: Define $\boldsymbol{\epsilon} = [\boldsymbol{\epsilon}_1^T, \ldots, \boldsymbol{\epsilon}_N^T]^T \in \mathbb{R}^{3N}$ where $\boldsymbol{\epsilon}_i = \hat{\boldsymbol{e}}_i - \boldsymbol{e}_i - (\hat{\boldsymbol{c}}_i - \boldsymbol{R}_Z(\phi_i)\boldsymbol{R}(-\theta_i)\boldsymbol{c}_i^*) \in \mathbb{R}^3$ and $\boldsymbol{\delta} = [\boldsymbol{\delta}_1^T, \ldots, \boldsymbol{\delta}_N^T]^T \in \mathbb{R}^{3N}$ where $\boldsymbol{\delta}_i = \hat{v}_i[\cos\hat{\phi}_i\cos\hat{\theta}_i, \sin\hat{\phi}_i\cos\hat{\theta}_i, \sin\hat{\theta}_i]^T - \dot{\boldsymbol{r}}_0 \in \mathbb{R}^3$ for $i \in \mathcal{N}$. Then, (11) can be expressed as

$$\dot{\boldsymbol{\epsilon}} = -k_7(\bar{\boldsymbol{L}} \otimes \boldsymbol{I}_3)\boldsymbol{\epsilon} + \boldsymbol{\delta}. \tag{12}$$

Then, we can derive that

$$\begin{aligned}\|\boldsymbol{\delta}_i\| &= \left\|(\hat{v}_i - v_0)\boldsymbol{u}\left(\hat{\phi}_i, \hat{\theta}_i\right) - v_0\left(\boldsymbol{u}(\phi_0,\theta_0) - \boldsymbol{u}\left(\hat{\phi}_i,\hat{\theta}_i\right)\right)\right\| \\ &\leq \left\|\hat{v}_i - v_0\right\| + |v_0|\left\|\boldsymbol{u}(\phi_0,\theta_0) - \boldsymbol{u}\left(\hat{\phi}_i,\hat{\theta}_i\right)\right\| \\ &\leq \left\|\hat{v}_i - v_0\right\| + l_1\left\|\phi_0 - \hat{\phi}_i\right\| + l_2\left\|\theta_0 - \hat{\theta}_i\right\|\end{aligned} \tag{13}$$

where $l_1, l_2 > 0$ are Lipschitz constants. The last inequality is by boundedness of v_0 and Lipschitz continuous of $\boldsymbol{u}(\phi,\theta)$. As a result, $\boldsymbol{\delta} \to \boldsymbol{0}$ exponentially follows Lemma 1 and $-(\bar{\boldsymbol{L}} \otimes \boldsymbol{I}_3)$ is Hurwitz, which makes $\boldsymbol{\epsilon}$ converge to $\boldsymbol{0}$ exponentially. Moreover, since $\hat{\boldsymbol{c}}_i \to \boldsymbol{R}_Z(\phi_i)\boldsymbol{R}(-\theta_i)\boldsymbol{c}_i^*$ exponentially from Lemma 2, we have $\hat{\boldsymbol{e}}_i \to \boldsymbol{e}_i$ exponentially. ■

Recall that our objective is to design v_i, ω_i, and u_i to steer $\boldsymbol{e}_i$ to $\boldsymbol{0}$. With transformation (5), we may turn to design $\ddot{\boldsymbol{r}}_i$. Now, although $\boldsymbol{e}_i$ is not accessible, we have derived the estimation $\hat{\boldsymbol{e}}_i$, which will converge to $\boldsymbol{e}_i$. As a result, in the following, a design of $\ddot{\boldsymbol{r}}_i$ such that $\hat{\boldsymbol{e}}_i$ converges to $\boldsymbol{0}$ will be proposed.

C. Design for $\ddot{\boldsymbol{r}}_i$

To design $\ddot{\boldsymbol{r}}_i$, we consider second-order dynamics, $\ddot{\hat{\boldsymbol{e}}}_i + \gamma_1\dot{\hat{\boldsymbol{e}}}_i + \gamma_2\hat{\boldsymbol{e}}_i = 0$, where $\gamma_1, \gamma_2 > 0$ are arbitrary constants. Then, the following theorem is proposed.

Theorem 1: With Lemmas 1–3, and the following design:

$$\begin{aligned}\ddot{\boldsymbol{r}}_i &= \ddot{\hat{\boldsymbol{c}}}_i + k_7\sum_{j\in\bar{N}_i}\left[\dot{\hat{\boldsymbol{e}}}_j - \dot{\hat{\boldsymbol{e}}}_i + \dot{\boldsymbol{r}}_j - \dot{\boldsymbol{r}}_i + \dot{\hat{\boldsymbol{c}}}_i - \dot{\hat{\boldsymbol{c}}}_j\right] \\ &\quad + \dot{\hat{v}}_i\left[\cos\hat{\phi}_i\cos\hat{\theta}_i, \sin\hat{\phi}_i\cos\hat{\theta}_i, \sin\hat{\theta}_i\right]^T + \gamma_1\dot{\hat{\boldsymbol{e}}}_i \\ &\quad + \dot{\hat{\phi}}_i\hat{v}_i\left[-\sin\hat{\phi}_i\cos\hat{\theta}_i, \cos\hat{\phi}_i\cos\hat{\theta}_i, 0\right]^T + \gamma_2\hat{\boldsymbol{e}}_i \\ &\quad + \dot{\hat{\theta}}_i\hat{v}_i\left[-\cos\hat{\phi}_i\sin\hat{\theta}_i, -\sin\hat{\phi}_i\sin\hat{\theta}_i, \cos\hat{\theta}_i\right]^T\end{aligned} \tag{14}$$

for $i \in \mathcal{N}$, $\hat{\boldsymbol{e}}_i$ will converge to $\boldsymbol{0}$ exponentially.

Proof: The proposed law can be rearranged into second-order relation, $\ddot{\hat{\boldsymbol{e}}}_i + \gamma_1\dot{\hat{\boldsymbol{e}}}_i + \gamma_2\hat{\boldsymbol{e}}_i = 0$, which states the exponential convergence by the Hurwitz property. ■

Then, once $\ddot{\boldsymbol{r}}_i$ is designed, the physical control inputs v_i, ω_i, and u_i, can be obtained from (5).

Remark 1: The method proposed in this section can achieve natural tracking since we introduce the relative description along with the estimation process to retrieve information at correct timing, preknown, and online, respectively. That is, we decouple the formation object so that the online feature is captured in the progress of formation, for example, the orientation of formation pattern for natural tracking. Moreover, suppose we "turn off" (8) and (9), that is, fix all $\hat{\phi}_i$ and $\hat{\theta}_i$ to some constants, then the proposed method will degenerate to the tracking with fixed orientation case, as in [15], [16], and [22], to name a few.

V. Input Saturation

By Theorem 1 with transformation (5), it seems that our problem can be solved. However, the issue of singularity may occur while applying the relation (5). We can make some arguments on the velocity v_i as in [39] to avoid singularities, for example, $v_i \neq 0\ \forall t$. However, even in such singularity-free case, small velocity v_i may still lead to large control inputs ω_i and u_i. As a result, in this section, we introduce the local viewpoints of agents for the saturation design.

To obtain more insights, first note that (14) is originated from the mass-point double integrator model while model (3) is subject to nonholonomic constraints. As a result, when transforming between two models, the control inputs are coupled as in (5). In order to decouple the inputs, we observe the geometrical relation between $\hat{\boldsymbol{e}}_i$ and local frame of agent-i. In Fig. 4, $\hat{\boldsymbol{e}}_i$ is decomposed into $\tilde{x}_i$, $\tilde{y}_i$, and $\tilde{z}_i$, which are closely related to inputs v_i, ω_i, and u_i, respectively. More precisely, as indicated by the geometric relation, the speed adjustment v_i may directly compensate $\tilde{x}_i$, while $\tilde{y}_i$ and $\tilde{z}_i$ would try to pull the agent in yaw and pitch direction, which correspond to ω_i and u_i, respectively. As a result, instead of considering $\hat{\boldsymbol{e}}_i$ directly, we transform it into $[\tilde{x}_i, \tilde{y}_i, \tilde{z}_i]^T \in \mathbb{R}^3$ w.r.t local frame by

$$\left[\tilde{x}_i, \tilde{y}_i, \tilde{z}_i\right]^T = \boldsymbol{R}_Y(\theta_i)\boldsymbol{R}_Z(-\phi_i)\hat{\boldsymbol{e}}_i \tag{15}$$

for $i \in \mathcal{N}$. Next, recall the notation $\boldsymbol{u}(\phi,\theta)$ defined as $[\cos\phi\cos\theta, \sin\phi\cos\theta, \sin\theta]^T$, we will derive the

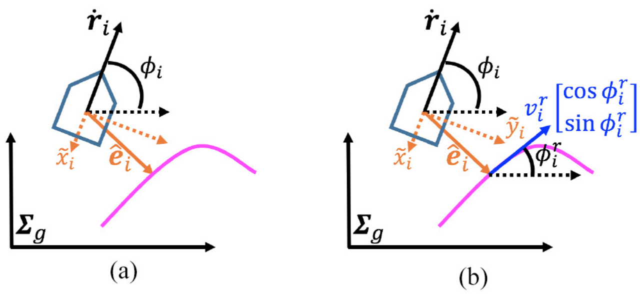

Fig. 4. Since the graph interpretation for 3-D transformation is not easy to observe, we provide concise 2-D case where the variables are illustrated. With the 2-D graphical interpretations, 3-D case is defined rigorously by (15) and (16). (a) Transformation of $\hat{\boldsymbol{e}}_k$. (b) Reference heading ϕ_k^r.

transformation of heading errors. Note that from Lemmas 1 and 2, we have $\hat{v}_i\boldsymbol{u}(\hat{\phi}_i,\hat{\theta}_i) + \dot{\hat{\boldsymbol{c}}}_i$ that exponentially converges to $v_0\boldsymbol{u}(\phi_0,\theta_0)+(d/dt)(\boldsymbol{R}_Z(\phi_0)\boldsymbol{R}_Y(-\theta_0)\boldsymbol{c}_i^*)$, which is the desired velocity of agent-i, the derivative of (4). As a result, $\hat{v}_i\boldsymbol{u}(\hat{\phi}_i,\hat{\theta}_i)+\dot{\hat{\boldsymbol{c}}}_i$ provides available information of desired headings. For consistency, describe $\hat{v}_i\boldsymbol{u}(\hat{\phi}_i,\hat{\theta}_i)+\dot{\hat{\boldsymbol{c}}}_i$ in model form as $v_i^r\boldsymbol{u}(\phi_i^r,\theta_i^r)$. With the above statements, we then define the transformed heading errors, $[\tilde{\phi}_i,\tilde{\theta}_i]^T \in \mathbb{R}^2$, by

$$\left[\tilde{\phi}_i,\tilde{\theta}_i\right]^T = \left[\phi_i^r-\phi_i,\theta_i^r-\theta_i\right]^T \tag{16}$$

for $i \in \mathcal{N}$. In the following, with the transformation, we can now directly design v_i, ω_i, and u_i, to steer (15) and (16) to $\mathbf{0}$.

The error dynamics of $[\tilde{x}_i,\tilde{y}_i,\tilde{z}_i]^T$ is derived as

$$\begin{aligned}\begin{bmatrix}\dot{\tilde{x}}_i\\ \dot{\tilde{y}}_i\\ \dot{\tilde{z}}_i\end{bmatrix} &= u_i\dot{\boldsymbol{R}}_Y(\theta_i)\boldsymbol{R}_Z(-\phi_i)\hat{\boldsymbol{e}}_i + (-\omega_i)\boldsymbol{R}_Y(\theta_i)\dot{\boldsymbol{R}}_Z(-\phi_i)\hat{\boldsymbol{e}}_i\\ &\quad+\boldsymbol{R}_Y(\theta_i)\boldsymbol{R}_Z(-\phi_i)\dot{\hat{\boldsymbol{e}}}_i \qquad (17)\\ &= u_i\begin{bmatrix}0&0&1\\0&0&0\\-1&0&0\end{bmatrix}\begin{bmatrix}\tilde{x}_i\\ \tilde{y}_i\\ \tilde{z}_i\end{bmatrix} + \omega_i\begin{bmatrix}0&c\theta_i&0\\-c\theta_i&0&s\theta_i\\0&-s\theta_i&0\end{bmatrix}\begin{bmatrix}\tilde{x}_i\\ \tilde{y}_i\\ \tilde{z}_i\end{bmatrix}\\ &\quad+v_i^r\begin{bmatrix}\left(c\tilde{\phi}_i-1\right)c\theta_i c\theta_i^r+c\tilde{\theta}_i\\ s\tilde{\phi}_i c\theta_i^r\\ \left(1-c\tilde{\phi}_i\right)s\theta_i c\theta_i^r+s\tilde{\theta}_i\end{bmatrix} - \begin{bmatrix}v_i\\0\\0\end{bmatrix} + \begin{bmatrix}o_i^x\\ o_i^y\\ o_i^z\end{bmatrix} \qquad (18)\end{aligned}$$

for $i \in \mathcal{N}$, where $[o_i^x,o_i^y,o_i^z]^T$, related to the last term of (11), is $k_7\boldsymbol{R}_Y(\theta_i)\boldsymbol{R}_Z(-\phi_i)\sum_{j\in\bar{N}_i}(\hat{\boldsymbol{e}}_j-\hat{\boldsymbol{e}}_i+\boldsymbol{r}_j-\boldsymbol{r}_i+\hat{\boldsymbol{c}}_i-\hat{\boldsymbol{c}}_j)$. Here, $s\tilde{\phi}_i$ is shorthand for $\sin\tilde{\phi}_i$, $c\theta_i^r$ is shorthand for $\cos\theta_i^r$, and so on. For the dynamics of $[\tilde{\phi}_i,\tilde{\theta}_i]^T$, it is derived as

$$\begin{bmatrix}\dot{\tilde{\phi}}_i\\ \dot{\tilde{\theta}}_i\end{bmatrix} = \begin{bmatrix}\omega_i^r-\omega_i\\ u_i^r-u_i\end{bmatrix} \tag{19}$$

for $i \in \mathcal{N}$, where ω_i^r and u_i^r are $\dot{\phi}_i^r$ and $\dot{\theta}_i^r$, respectively.

By the transformation, we will design constrained control inputs, $v_i \in [v_-,v_+]$, $\omega_i \in [\omega_-,\omega_+]$, $u_i \in [u_-,u_+]$, such that $[\tilde{x}_i,\tilde{y}_i,\tilde{z}_i,\tilde{\phi}_i,\tilde{\theta}_i]^T$ converges to $\mathbf{0}$, for $i \in \mathcal{N}$, where v_-, ω_-, u_- are negative while v_+, ω_+, and u_+ are positive.

Remark 2: Suppose θ_i, θ_i^r, $\tilde{\theta}_i$, $\tilde{z}_i$, and u_i all equal to 0, that is, when considering 2-D case, (18) and (19) degenerate into the case derived in [41]

$$\begin{bmatrix}\dot{\tilde{x}}_i\\ \dot{\tilde{y}}_i\\ \dot{\tilde{\phi}}_i\end{bmatrix} = \begin{bmatrix}v_i^r\cos\tilde{\phi}_i-v_i\\ v_i^r\sin\tilde{\phi}_i\\ \omega_i^r-\omega_i\end{bmatrix} + \begin{bmatrix}o_i^x\\ o_i^y\\ 0\end{bmatrix}.$$

Before illustrating the design of saturated inputs, we define some notations and provide mild assumptions to make the theorem compact. To achieve natural tracking (4), agent-i seeks to follow smooth signal $\boldsymbol{r}_0+\boldsymbol{R}_Z(\phi_0)\boldsymbol{R}_Y(-\theta_0)\boldsymbol{c}_i^*$. Correspondingly, the desired velocity is $(d/dt)(\boldsymbol{r}_0+\boldsymbol{R}_Z(\phi_0)\boldsymbol{R}_Y(-\theta_0)\boldsymbol{c}_i^*)$. For consistency, we express it in unicycle form as $v_i^*\boldsymbol{u}(\phi_i^*,\theta_i^*)$. It is clear that the desired signals v_i^*, $\omega_i^*(=\dot{\phi}_i^*)$ and $u_i^*(=\dot{\theta}_i^*)$ should be bounded. Without loss of generality, suppose that they are constrained in $\mathcal{V}^*=[v_-^*,v_+^*]$, $\mathcal{W}^*=[\omega_-^*,\omega_+^*]$, and $\mathcal{U}^*=[u_-^*,u_+^*]$, respectively, for all agents, where v_-^*, ω_-^*, u_-^* are negative, while v_+^*, ω_+^*, and u_+^* are positive. Practically, we assume that $v_-^*=-v_+^*$, $\omega_-^*=-\omega_+^*$, and $u_-^*=-u_+^*$, in the following. Then, we provide two mild assumptions.

Assumption 1: $\mathcal{V}^*\subsetneq\mathcal{V}$, $\mathcal{W}^*\subsetneq\mathcal{W}$, $\mathcal{U}^*\subsetneq\mathcal{U}$, where $\mathcal{V}$, $\mathcal{W}$, and $\mathcal{U}$ are $[v_-,v_+]$, $[\omega_-,\omega_+]$, and $[u_-,u_+]$, respectively.

Assumption 2: $v_i^*\neq 0\ \forall t$, for $i\in\mathcal{N}$.

Remark 3: If Assumption 1 is violated, then agents may never take the desired trajectory due to the permanent slower motions. Assumption 2 indicates that each "desired" trajectory has no singularity. Note that it is imposed on the desired trajectory and hence reasonable.

Since we are going to propose the theorem for saturated design, we define the saturation function, which projects scalar c into the saturated interval $\mathcal{I}=[\mathcal{I}^-,\mathcal{I}^+]$, as

$$\mathbf{sat}_{\mathcal{I}}(c) = \begin{cases}\mathcal{I}^-, & \text{if } c<\mathcal{I}^-\\ c, & \text{if } \mathcal{I}^-\le c\le\mathcal{I}^+\\ \mathcal{I}^+, & \text{if } c>\mathcal{I}^+.\end{cases}$$

Then, the design of *constrained* control inputs, which achieves natural tracking, is proposed in the following main theorem.

Theorem 2: Assume Assumptions 1 and 2. With Lemmas 1–3, and the following proposed constrained control laws:

$$\begin{aligned}v_i &= \boldsymbol{sat}_{\mathcal{V}^*}\left(v_i^r\right)\left[\left(\cos\tilde{\phi}_i-1\right)\cos\theta_i\cos\theta_i^r+1\right]\\ &\quad+k_8\boldsymbol{sat}_{\mathcal{X}}(\tilde{x}_i) \qquad (20)\end{aligned}$$

$$\begin{aligned}\omega_i &= \boldsymbol{sat}_{\mathcal{W}^*}\left(\omega_i^r\right)+k_9\frac{\tilde{y}_i\boldsymbol{sat}_{\mathcal{V}^*}\left(v_i^r\right)\cos\frac{\tilde{\phi}_i}{2}\cos\theta_i^r}{\sqrt{1+\tilde{x}_i^2+\tilde{y}_i^2+\tilde{z}_i^2}}\\ &\quad+k_{10}\sin\frac{\tilde{\phi}_i}{2}+k_9\frac{\tilde{z}_i\boldsymbol{sat}_{\mathcal{V}^*}\left(v_i^r\right)\sin\frac{\tilde{\phi}_i}{2}\sin\theta_i\cos\theta_i^r}{\sqrt{1+\tilde{x}_i^2+\tilde{y}_i^2+\tilde{z}_i^2}} \qquad (21)\end{aligned}$$

$$\begin{aligned}u_i &= \boldsymbol{sat}_{\mathcal{U}^*}\left(u_i^r\right)+k_{11}\frac{\tilde{z}_i\boldsymbol{sat}_{\mathcal{V}^*}\left(v_i^r\right)\cos\frac{\tilde{\theta}_i}{2}}{\sqrt{1+\tilde{x}_i^2+\tilde{y}_i^2+\tilde{z}_i^2}}\\ &\quad+k_{12}\sin\frac{\tilde{\theta}_i}{2}-k_{11}\frac{\tilde{x}_i\boldsymbol{sat}_{\mathcal{V}^*}\left(v_i^r\right)\sin\frac{\tilde{\theta}_i}{2}}{\sqrt{1+\tilde{x}_i^2+\tilde{y}_i^2+\tilde{z}_i^2}} \qquad (22)\end{aligned}$$

for $i\in\mathcal{N}$, the error state $[\tilde{x}_i,\tilde{y}_i,\tilde{z}_i,\tilde{\phi}_i,\tilde{\theta}_i]^T$ will converge to $\mathbf{0}$. Note that $\mathcal{X}$ and $k_i>0$, $i=8,\ldots,12$ are design parameters such that $v_i\in\mathcal{V}$, $\omega_i\in\mathcal{W}$, and $u_i\in\mathcal{U}$.

Proof: Rewrite (18) into

$$\begin{bmatrix}\dot{\tilde{x}}_i\\ \dot{\tilde{y}}_i\\ \dot{\tilde{z}}_i\end{bmatrix} = u_i\begin{bmatrix}0&0&1\\0&0&0\\-1&0&0\end{bmatrix}\begin{bmatrix}\tilde{x}_i\\ \tilde{y}_i\\ \tilde{z}_i\end{bmatrix} + \omega_i\begin{bmatrix}0&c\theta_i&0\\-c\theta_i&0&s\theta_i\\0&-s\theta_i&0\end{bmatrix}\begin{bmatrix}\tilde{x}_i\\ \tilde{y}_i\\ \tilde{z}_i\end{bmatrix}$$
$$+\ \boldsymbol{sat}_{\mathcal{V}^*}(v_i^r)\begin{bmatrix}\left(c\tilde{\phi}_i-1\right)c\theta_i c\theta_i^r + c\tilde{\theta}_i\\ s\tilde{\phi}_i c\theta_i^r\\ \left(1-c\tilde{\phi}_i\right)s\theta_i c\theta_i^r + s\tilde{\theta}_i\end{bmatrix} - \begin{bmatrix}v_i\\0\\0\end{bmatrix} + \underbrace{\begin{bmatrix}o_i^x\\o_i^y\\o_i^z\end{bmatrix}}_{:=\boldsymbol{o}_i\in\mathbb{R}^3}$$
$$+\ \underbrace{\left(v_i^r - \boldsymbol{sat}_{\mathcal{V}^*}(v_i^r)\right)\begin{bmatrix}\left(c\tilde{\phi}_i-1\right)c\theta_i c\theta_i^r + c\tilde{\theta}_i\\ s\tilde{\phi}_i c\theta_i^r\\ \left(1-c\tilde{\phi}_i\right)s\theta_i c\theta_i^r + s\tilde{\theta}_i\end{bmatrix}}_{:=\boldsymbol{s}_i^v\in\mathbb{R}^3}, \tag{23}$$

where $\boldsymbol{o}_i$ and $\boldsymbol{s}_i^v$ are the perturbed errors from observer and saturation constraints, respectively. Similarly, rewrite (19) into

$$\begin{bmatrix}\dot{\tilde{\phi}}_i\\ \dot{\tilde{\theta}}_i\end{bmatrix} = \begin{bmatrix}\boldsymbol{sat}_{\mathcal{W}^*}\left(\omega_i^r\right)-\omega_i\\ \boldsymbol{sat}_{\mathcal{U}^*}\left(u_i^r\right)-u_i\end{bmatrix} + \underbrace{\begin{bmatrix}\omega_i^r - \boldsymbol{sat}_{\mathcal{W}^*}\left(\omega_i^r\right)\\ u_i^r - \boldsymbol{sat}_{\mathcal{U}^*}\left(u_i^r\right)\end{bmatrix}}_{:=\boldsymbol{s}_i^h\in\mathbb{R}^2} \tag{24}$$

where $\boldsymbol{s}_i^h$ is the perturbed heading error due to saturation.

To prove the asymptotic convergence of the perturbed system (23) and (24), we first prove the exponential convergences of the perturbed errors, $\boldsymbol{o}_i$, $\boldsymbol{s}_i^v$, and $\boldsymbol{s}_i^h$. Then, the unperturbed system, with $\boldsymbol{o}_i = \boldsymbol{s}_i^v = \boldsymbol{s}_i^h \equiv \mathbf{0}$, is proved asymptotically stable. Last, we show the boundedness of the perturbed system. With the above three steps, a lemma in [42] can be utilized to prove the asymptotic convergence of overall perturbed system (23) and (24). As a result, the theorem is then proved.

For the convergences of $\boldsymbol{o}_i$, $\boldsymbol{s}_i^v$, and $\boldsymbol{s}_i^h$, we base on Lemmas 1–3. Since Lemmas 2 and 3 state the convergences of $\hat{\boldsymbol{c}}_i$ and $\hat{\boldsymbol{e}}_i$, the exponential convergence of $\boldsymbol{o}_i$ follows. As for convergence of $\boldsymbol{s}_i^h$, based on Lemmas 1 and 2, the estimated $v_i^r\boldsymbol{u}(\phi_i^r, \theta_i^r)$ converges exponentially to desired velocity $v^*\boldsymbol{u}(\phi^*, \theta^*)$. As a result, ω_i^r and u_i^r will fall into $\mathcal{W}^*$ and $\mathcal{U}^*$ exponentially, respectively. Since sin and cos are bounded, the exponential convergence of $\boldsymbol{s}_i^v$ can be proved similarly as $\boldsymbol{s}_i^h$.

Then, to prove the asymptotic convergence of the unperturbed system, we propose a Lyapunov function candidate

$$V_i = \sqrt{1+\tilde{x}_i^2+\tilde{y}_i^2+\tilde{z}_i^2} - 1 + \frac{4}{k_9}\left(1-\cos\frac{\tilde{\phi}_i}{2}\right) + \frac{4}{k_{11}}\left(1-\cos\frac{\tilde{\theta}_i}{2}\right).$$

After differentiating along the unperturbed system and substituting the control laws (20)–(22), we have

$$\dot{V}_i = -\frac{k_8\tilde{x}_i\boldsymbol{sat}_{\mathcal{X}}(\tilde{x}_i)}{\sqrt{1+\tilde{x}_i^2+\tilde{y}_i^2+\tilde{z}_i^2}} - k_{10}\sin^2\frac{\tilde{\phi}_i}{2} - k_{12}\sin^2\frac{\tilde{\theta}_i}{2}.$$

Since the function $f(x) := x\boldsymbol{sat}_{\mathcal{I}}(x)$ is positive definite and uniformly continuous, we have $\dot{V}_i \le 0$, V_i lower bounded, and $\dot{V}_i$ uniformly continuous. As a result, by the Lyapunov-like lemma, $\dot{V}_i \to 0$ is guaranteed with $\tilde{x}_i, \tilde{\phi}_i, \tilde{\theta}_i \to 0$. Then, since $\tilde{\theta}_i \to 0$ and u_i is uniformly continuous, we apply Barbalat's lemma to obtain $u_i \to 0$, which implies $\tilde{z}_i \to 0$. Similarly, we apply Barbalat's lemma to ω_i, which leads to $\tilde{y}_i \to 0$. Thus, the unperturbed system is proved asymptotically stable.

The last step is to prove the boundedness of overall system (23) and (24). Then, the lemma in [42] can be applied to prove the asymptotic convergence of it. Consider V_i and differentiate along overall system, then we have

$$\dot{V}_i = -\frac{k_8\tilde{x}_i\boldsymbol{sat}_{\mathcal{X}}(\tilde{x}_i)}{\sqrt{1+\tilde{x}_i^2+\tilde{y}_i^2+\tilde{z}_i^2}} - k_{10}\sin^2\frac{\tilde{\phi}_i}{2} - k_{12}\sin^2\frac{\tilde{\theta}_i}{2} + \nabla V_i^T\left[\left[\boldsymbol{o}_i+\boldsymbol{s}_i^v\right]^T, \boldsymbol{s}_i^{h^T}\right]^T \tag{25}$$

with $\nabla V_i = [(\tilde{x}_i/p_i), (\tilde{y}_i/p_i), (\tilde{z}_i/p_i), (2/k_9)\sin(\tilde{\phi}_i/2), (2/k_{11})\sin(\tilde{\theta}_i/2)]^T \in \mathbb{R}^5$, where $p_i = \sqrt{1+\tilde{x}_i^2+\tilde{y}_i^2+\tilde{z}_i^2}$. Thus, we have loose bound $\|\nabla V_i\| \le \sqrt{1+(4/k_9^2)+(4/k_{11}^2)}(:=\alpha)$. Then, following (25), we have

$$\dot{V}_i \le \alpha\left\|\left[\boldsymbol{o}_i+\boldsymbol{s}_i^v\right]^T, \boldsymbol{s}_i^{h^T}\right\| \le \alpha\left(\|\boldsymbol{o}_i\| + \left\|\boldsymbol{s}_i^v\right\| + \left\|\boldsymbol{s}_i^h\right\|\right). \tag{26}$$

Integrating both sides from 0 to t, we obtain

$$\int_0^t \dot{V}_i d\tau \le \alpha\int_0^t \|\boldsymbol{o}_i\| + \left\|\boldsymbol{s}_i^v\right\| + \left\|\boldsymbol{s}_i^h\right\| d\tau. \tag{27}$$

Since $\|\boldsymbol{o}_i\|, \|\boldsymbol{s}_i^v\|, \|\boldsymbol{s}_i^h\| \to 0$ exponentially, the right-hand side of (27) is integrable, say $\bar{\alpha}$. As a result, we have

$$V_i(t) \le V_i(0) + \bar{\alpha} \tag{28}$$

which states the boundedness of overall system (23) and (24).

With above three steps, the asymptotic convergence of the overall system follows the lemma in [42]. That is, natural tracking (4) is achieved by proposed design with saturation. ■

Remark 4: In this remark, we will provide some design guidelines for $\mathcal{X}$ and k_i, $i = 8, \ldots, 12$. By Assumption 1, we may define constants $k_v := \min(v_-^* - v_-, v_+ - v_+^*)$, $k_\omega := \min(\omega_-^* - \omega_-, \omega_+ - \omega_+^*)$, $k_u := \min(u_-^* - u_-, u_+ - u_+^*)$, which are all positive. Since $(\cos\tilde{\phi}_i - 1)\cos\theta_i\cos\theta_i^r + 1 \in [-1, 1]$, if we make $k_8\ \boldsymbol{sat}_{\mathcal{X}}(\cdot) \le k_v$, then v_i is guaranteed within $\mathcal{V}$. As for ω_i, the sum of second, third, and fourth term on the right-hand side of (21) is bounded by $2k_9v_+^* + k_{10}$. Thus, we choose k_9 and k_{10} such that $2k_9v_+^* + k_{10} \le k_\omega$, then ω_i is bounded in $\mathcal{W}$. Similarly, we choose k_{11} and k_{12} to ensure $2k_{11}v_+^* + k_{12} \le k_u$, then u_i is bounded in $\mathcal{U}$.

Remark 5: As the design guideline mentioned in Remark 4, k_8 and interval $\mathcal{X}$, k_9 and k_{10}, k_{11} and k_{12}, are three reciprocal inhibition groups, for example, as k_9 arises, k_{10} requires decreasing, since $2k_9v_+^* + k_{10}$ is bounded by the constant k_ω. Among those, k_9 and k_{11} weight the turning force resulted from position errors, while k_{10} and k_{12} feedback the heading errors. That is, they tradeoff between position and heading errors. As for k_8 and $\mathcal{X}$, when selecting larger feedback gain k_8, the interval $\mathcal{X}$ will be smaller, which implies that the saturation condition is active more often.

Remark 6: In this remark, we provide an insight of the overall proposed scheme. First, by Lemmas 1–3, agents "cooperatively" determine the indicated target directions $\hat{\boldsymbol{e}}_i$, for $i \in \mathcal{N}$. Then, each agent "locally" decides its control inputs

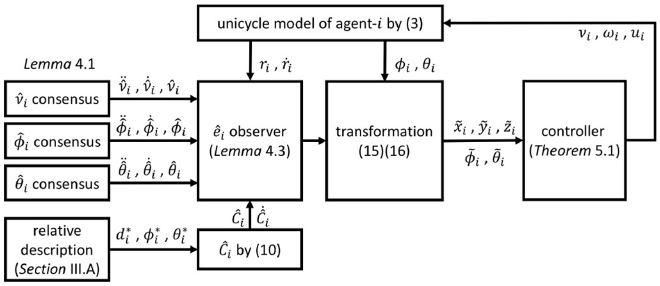

Fig. 5. Block diagram of control process and signal flow.

with consideration of saturation to move toward the target. The two-phase scheme is similar to the solution of classical robotic navigation, where a global planner is first applied to obtain rough plan, then a local planner adjusts the control inputs based on local conditions.

At the end of this section, we provide a block diagram to illustrate the overall design and signal flow in Fig. 5.

VI. Extensions to the Proposed Design

Our proposed design that achieves natural tracking with saturated inputs can be extended with some attractive functionalities. In the following, we will demonstrate extensions to pattern-varying formation and switching communication case.

A. Pattern-Varying Formation

Pattern-varying formation states that the desired pattern which the MAS forms is varying. With the ability, the formation can online adapt to the environments and avoid obstacles. Here, we consider a simpler case that the nominal (original) pattern, $\{d_i^*, \phi_i^*, \theta_i^*\}$, can be scaled, skewed, or rotated by a smooth transformation command $\boldsymbol{G}_0(t) \in \mathbb{R}^{3\times 3}$, for example

$$\boldsymbol{G}_{0,\text{scale}} : \begin{bmatrix} 3+\cos t & 0 & 0 \\ 0 & 2 & 0 \\ 0 & 0 & 1 \end{bmatrix}, \boldsymbol{G}_{0,\text{skew}} : \begin{bmatrix} 1 & 2\sin t & 0 \\ 0 & 1 & 0 \\ 0 & 0 & 1 \end{bmatrix}.$$

With proposed relative description $\{d_i^*, \phi_i^*, \theta_i^*\}$, apply transformation $\boldsymbol{G}_0$ is rather simple, by replacing $\boldsymbol{c}_i^*$ with $\boldsymbol{G}_0\boldsymbol{c}_i^*$. For example, the original objective (4) becomes

$$\boldsymbol{r}_i \to \boldsymbol{r}_0 + \boldsymbol{R}_Z(\phi_0)\boldsymbol{R}_Y(-\theta_0)\boldsymbol{G}_0\boldsymbol{c}_i^*. \tag{29}$$

Correspondingly, we modify (10) into

$$\hat{\boldsymbol{c}}_i = \boldsymbol{R}_Z\left(\hat{\phi}_i\right)\boldsymbol{R}_Y\left(-\hat{\theta}_i\right)\boldsymbol{G}_0\boldsymbol{c}_i^*. \tag{30}$$

Then, Theorem 2 now achieves pattern-varying formation in addition to natural tracking, though the meaning of $\hat{\boldsymbol{c}}_i$ differs.

B. Switching Communication Graph

Communication plays a crucial role in MAS. For example, if agents can, in addition, receive the reference signal v_0, ϕ_0, and θ_0, then the MAS can converge faster. To relieve more communication restrictions, more investigations are required, for example, switching communications. Switching communications means that the communication graph is time varying. Since communication range is restricted due to the signal strength in reality, communicating with closer neighbors while moving is more feasible. Here, we suppose that the MAS switches within s strongly connected graphs, denoted as set $S = \{1, \ldots, s\}$. Correspondingly, extended graphs are denoted as $\bar{\mathcal{G}}_i$ with Laplacian $\bar{\boldsymbol{L}}^i$, for $i \in S$.

Some technical terms are defined. The switching signal $\sigma(t) : [0, +\infty) \to S$ maps time t to a communication graph. The switching sequence $\{t_n\}_{n\in\mathbb{N}}$ is an increasing sequence, which indicates the time instants that communication graph alters. Given $\{t_n\}$, the dwell time τ_0 is the infimum of the switching period between two contiguous switching time instants, that is, $\tau_0 = \inf_{n\geq 1}(t_{n+1} - t_n)$. With $\sigma(t)$, we extend the notation $\bar{N}_i$ to $\bar{N}_i^{\sigma(t)}$ as the neighbor set at time t.

As mentioned in Remark 6, only the first stage, which covers Lemmas 1 and 3, is cooperatively designed. As a result, once we extend the two lemmas into switching communication case, Theorem 2 then achieves natural tracking under switching communications.

The extension of Lemma 1 to switching case is by replacing $\bar{N}_i$ with $\bar{N}_i^{\sigma(t)}$ in (7)–(9). Since it is a classical linear system switching case, the result is stated without proof, or one can refer to the later on proof of extension for Lemma 3. To make extension of Lemma 3 compact, we define some notations. Since $-k_7\bar{\boldsymbol{L}}^i \otimes \boldsymbol{I}_3$, for $i \in S$, is Hurwitz, we have

$$\left\| e^{-k_7(\bar{\boldsymbol{L}}^i\otimes \boldsymbol{I}_3)\tau} \right\| \leq \alpha e^{-\beta\tau} \tag{31}$$

for $\tau \geq 0$ and $i \in S$, where α and β are some positive constants. Besides, by the switching case of Lemma 1, the estimations still converge exponentially. As a result, $\boldsymbol{\delta}$ defined in (12) has

$$\|\boldsymbol{\delta}\| \leq \alpha_1 e^{-\beta_1 t} \tag{32}$$

for $t \geq 0$, where α_1 and β_1 are some positive constants.

Then, we may provide the switching case of Lemma 3 in the following. Moreover, a closed-form bound of the switching system with perturbation is derived.

Lemma 4: Suppose $\tau_0 > ([\ln(\alpha k_s)]/\beta)$, then the update law

$$\begin{aligned}\dot{\hat{\boldsymbol{e}}}_i = {} & \hat{v}_i\left[\cos\hat{\phi}_i\cos\hat{\theta}_i, \sin\hat{\phi}_i\cos\hat{\theta}_i, \sin\hat{\theta}_i\right]^T - \dot{\boldsymbol{r}}_i + \dot{\hat{\boldsymbol{c}}}_i \\ & + k_7 \sum_{j\in\bar{N}_i^{\sigma(t)}} \left[\hat{\boldsymbol{e}}_j - \hat{\boldsymbol{e}}_i + \boldsymbol{r}_j - \boldsymbol{r}_i + \hat{\boldsymbol{c}}_i - \hat{\boldsymbol{c}}_j\right]\end{aligned} \tag{33}$$

will drive $\hat{\boldsymbol{e}}_i \to \boldsymbol{e}_i$ exponentially, for $i \in \mathcal{N}$, where $k_7 > 0$. Here, $k_s = ([\max_{i\in S}\bar{\sigma}^i]/[\min_{i\in S}\underline{\sigma}^i])$, where $\bar{\sigma}^i$ and $\underline{\sigma}^i$ are the largest and smallest singular values of $\bar{\boldsymbol{L}}^i$, respectively.

Proof: Following proof in Lemma 3, then similarly, we have

$$\dot{\boldsymbol{\epsilon}} = -k_7\left(\bar{\boldsymbol{L}}^{\sigma(t)} \otimes \boldsymbol{I}_3\right)\boldsymbol{\epsilon} + \boldsymbol{\delta}. \tag{34}$$

To prove the exponential convergence of $\boldsymbol{\epsilon}$, we consider the harshest condition, that is, graph switches as fast as possible, and whenever switch occurs, the error enlarges by a maximum factor. That is, an impulsive signal occurs periodically and prompts the variable $\boldsymbol{\epsilon}$. Mathematically speaking

$$t_{n+1} - t_n = \Delta \tag{35}$$

$$\left\|\boldsymbol{\epsilon}\left(t_n^+\right)\right\| = k_s\left\|\boldsymbol{\epsilon}\left(t_n^-\right)\right\| \tag{36}$$

for $n \in \mathbb{N}$, where t_n^+ and t_n^- are right before and after switch instant t_n. Besides, Δ is the shortest period to be determined.

Integrate (34) from t_{n-1}^+ to t_n^- and apply (31)–(32), then

$$\begin{aligned}\left\|\boldsymbol{\epsilon}\left(t_n^-\right)\right\| \le\ & \alpha e^{-\beta\left(t_n^- - t_{n-1}^+\right)}\left\|\boldsymbol{\epsilon}\left(t_{n-1}^+\right)\right\| \\ & + \int_{t_{n-1}^+}^{t_n^-} \alpha e^{-\beta(t_n^- - \tau)}\alpha_1 e^{-\beta_1(\tau - t_0)}\|\boldsymbol{\delta}(t_0)\| d\tau \end{aligned} \tag{37}$$

$$\le \begin{cases} \text{if } \beta = \beta_1, \alpha e^{-\beta\left(t_n^- - t_{n-1}^+\right)}\left\|\boldsymbol{\epsilon}\left(t_{n-1}^+\right)\right\| + \alpha\alpha_1\|\boldsymbol{\delta}(t_0)\| \times \\ \quad \left(t_n^- - t_{n-1}^+\right)e^{-\beta\left(t_{n-1}^+ - t_0\right)}e^{-\beta\left(t_n^- - t_{n-1}^+\right)} \\ \text{if } \beta \neq \beta_1, \alpha e^{-\beta\left(t_n^- - t_{n-1}^+\right)}\left\|\boldsymbol{\epsilon}\left(t_{n-1}^+\right)\right\| + \alpha\alpha_1 \frac{\|\boldsymbol{\delta}(t_0)\|}{\beta - \beta_1} \times \\ \quad e^{-\beta_1\left(t_{n-1}^+ - t_0\right)}\left(e^{-\beta_1\left(t_n^- - t_{n-1}^+\right)} - e^{-\beta\left(t_n^- - t_{n-1}^+\right)}\right). \end{cases} \tag{38}$$

Apply (35), then we have

$$\left\|\boldsymbol{\epsilon}\left(t_n^-\right)\right\| \le \begin{cases} \text{if } \beta = \beta_1, \alpha e^{-\beta\Delta}\left\|\boldsymbol{\epsilon}\left(t_{n-1}^+\right)\right\| + \alpha\alpha_1 \times \\ \quad \|\boldsymbol{\delta}(t_0)\|\Delta e^{-n\beta\Delta} \\ \text{if } \beta \neq \beta_1, \alpha e^{-\beta\Delta}\left\|\boldsymbol{\epsilon}\left(t_{n-1}^+\right)\right\| + \alpha\alpha_1 \times \\ \quad \frac{\|\boldsymbol{\delta}(t_0)\|}{\beta - \beta_1} e^{-(n-1)\beta_1\Delta}\left(e^{-\beta_1\Delta} - e^{-\beta\Delta}\right). \end{cases} \tag{39}$$

With (36), we solve the recursion (39) and obtain

$$\left\|\boldsymbol{\epsilon}\left(t_n^-\right)\right\| \le \begin{cases} \text{if } \beta = \beta_1, \left(\alpha k_s e^{-\beta\Delta}\right)^n\|\boldsymbol{\epsilon}(t_0)\| + \|\boldsymbol{\delta}(t_0)\| \times \\ \quad \alpha\alpha_1 \frac{(\alpha k_s)^n - 1}{\alpha k_s - 1}\Delta e^{-n\beta\Delta} \\ \text{if } \beta \neq \beta_1, \left(\alpha k_s e^{-\beta\Delta}\right)^n\|\boldsymbol{\epsilon}(t_0)\| + \|\boldsymbol{\delta}(t_0)\| \times \\ \quad \frac{\alpha\alpha_1}{\beta - \beta_1}\frac{e^{-n\beta_1\Delta} - \left(\alpha k_s e^{-\beta\Delta}\right)^n}{e^{-\beta_1\Delta} - \alpha k_s e^{-\beta\Delta}}\left(e^{-\beta_1\Delta} - e^{-\beta\Delta}\right). \end{cases} \tag{40}$$

As a result, from (40), we conclude that $\Delta > ([\ln(\alpha k_s)]/\beta)$ is sufficient for $\|\boldsymbol{\epsilon}\|$ to converge exponentially to 0. ■

With the switching version of Lemmas 1 and 4, our proposed design (20)–(22) can achieve natural tracking in the switching communication scenario. Moreover, with the success of switching communications, the jointly strongly connected assumption can be further applied.

Remark 7: Recently, the more general concept of switching signal called mode-dependent average dwell-time (MDADT) switching is introduced in [43] and the results on stability and design of switched systems are improved. In [44]–[46], the switching mechanisms are further extended to the ones with transition probability (TP)-based MDADT, where the MDADT switching with probability is considered and the idea is widely applicable in many problems. Such switching mechanisms can be considered in the future research to help obtain more general results. In addition, communication delay is also an important issue in control of MASs, especially for the practical implementation of the system. Recently, there are many related results with consideration of delay, such as [47], where the necessary and sufficient condition for control of linear MAS is proposed. For nonlinear systems, some results about consensus are proposed, such as [48] and [49]. The design of robust maneuver controller with respect to communication delay has attracted much attention and is worthy of further investigation.

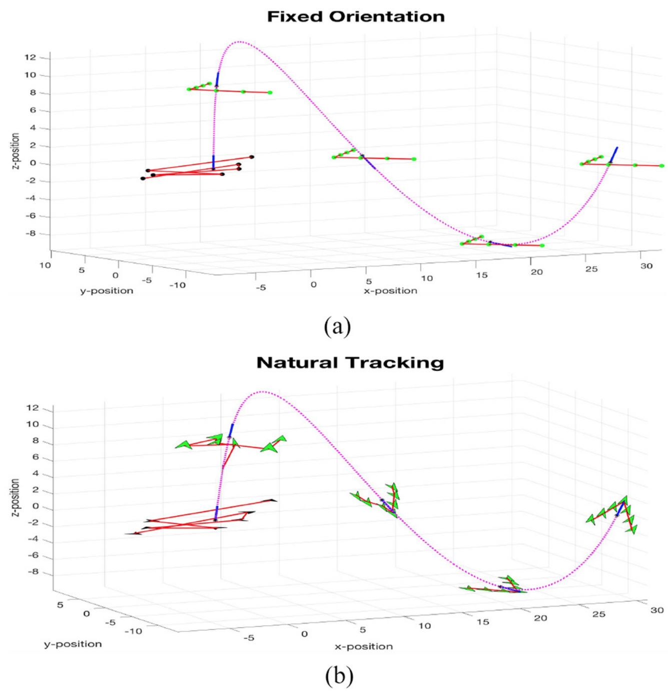

Fig. 6. Comparisons of maneuver control with and without heading alignment. (a) Formation with fixed orientation. (b) Formation with natural tracking.

VII. Simulation Results

In this section, four simulation examples are provided to validate the design performance. The first example compares with existing results of tracking in fixed orientation as in [9], [23], [32], and [33] and demonstrates our motivation of proposing natural tracking with nonholonomic constraints. In the second example, the advantage of 3-D formation over 2-D one is shown. In the third example, we compare the proposed saturation controller performing natural tracking with the existing results, which do not considering saturation and require additional conditions to achieve natural tracking, for example, [8] and [27]. Finally, we provide an illustration of heterogeneous hierarchical pattern-varying formation, which demonstrates the extensiveness of the proposed scheme.

Example 1: In this example, we compare the performance of our natural tracking design and the existing results that consider fixed orientation. We consider five agents and the desired formation pattern is the "check" shape. As mentioned in Section II-C, most existing papers considering the linear model (1) rely on the constant displacement $\boldsymbol{h}$ to describe the desired formation pattern, for example, [23] and [32]. However, the constant displacements lead to fixed orientation pattern as depicted in Fig. 6(a). The check pattern points permanently toward negative x-axis regardless of the moving direction along the reference trajectory (blue line), since the pregiven constant $\boldsymbol{h}$ completely determines the pattern. In general, this fixed orientation case is not suitable for applications, such as formation flying. In our design with *natural tracking*, the check pattern will point toward the moving direction. To evaluate headings, we progress from linear model (1) to nonlinear model (3) subject to nonholonomic constraints.

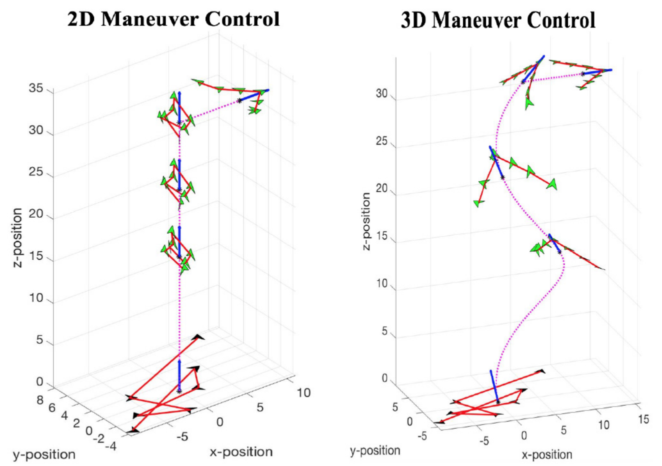

(a) (b)

Fig. 7. Comparisons between 2-D and 3-D formation maneuver control. (a) Formation maneuver in 2-D. (b) Formation maneuver in 3-D.

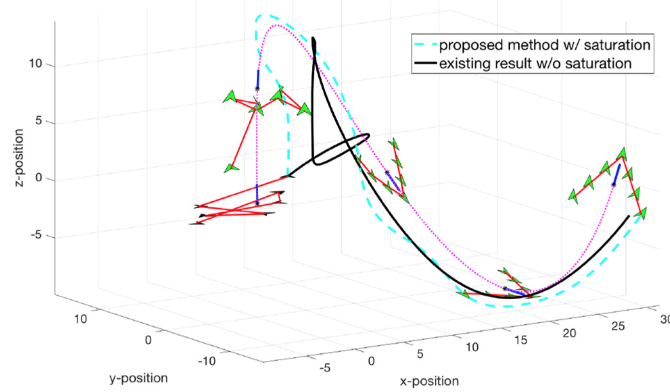

Fig. 8. Comparison of the trajectory with saturation (ours) and without saturation [27].

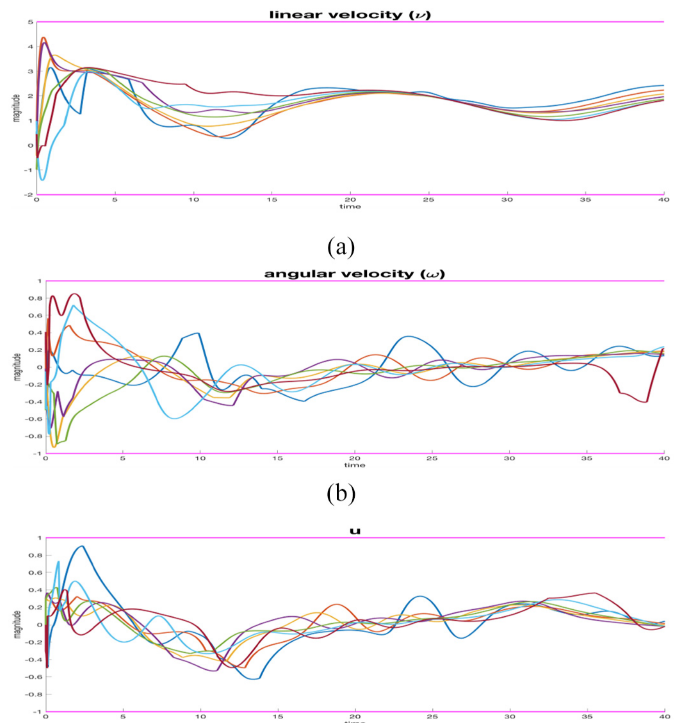

(a)

(b)

(c)

Fig. 9. Constrained input. (a) Linear velocity v. (b) Angular velocity ω. (c) Control u.

Besides, instead of being dominated by $\boldsymbol{h}$, we propose the preknown relative description in Section III-A along with an online estimation process (8) and (9) to compose the goal of headings, which facilitates the achievement of natural tracking. Our result is depicted in Fig. 6(b), where the formation pattern moves with the heading aligned to the moving direction compared with Fig. 6(a).

Example 2: In this example, we show the advantages of 3-D maneuver control compared with 2-D control. Consider five agents to form a planar check shape at a specified height, which is a common scenario for the UAVs. As depicted in Fig. 7(a), 2-D maneuver control will require agents to lift to the specific height, and then start to perform formation, where some transient distance is needed to complete formation. In opposite, with the 3-D maneuver control, agents can start forming during the lifting phase. As a result, when reaching at specific height, the system may have achieved the desired formation, as shown in Fig. 7(b). That is to say, 3-D maneuver can be more efficient and has advantage in the convergence distance over the 2-D control. Many of existing research with nonholonomic constraints focus on 2-D formation, while fewer results are studied in 3-D case. With capability of maneuver in 3-D space, it is foreseeable that formation can be designed more extensively than that in 2-D space.

Example 3: The merit of saturation control is demonstrated in this example. As mentioned in Example 1 that the time-invariant formation cannot achieve natural tracking, here we compare time-varying formation results with our saturation design. Recall the discussion in Section II-C, the time-varying formation requires the assumption of preknown and globally accessible signals to achieve natural tracking, which may violate the communication constraints. However, we adopt the assumption here in order to focus on the consideration of saturation. The existing results without saturation, such as [8] and [27], carried out by the nominal controller (2) may result in a quirky trajectory depicted in Fig. 8 by the black line, which is the trajectory of agent-1, and may not be implementable in practice. Whereas our method considering saturation is illustrated by the cyan dash line in Fig. 8, which is the trajectory of agent-1, and is much smoother. Our saturation control input is shown in Fig. 9, where the velocity and the angular velocity in yaw and pitch directions are constrained in a specified range, and results in a more practical trajectory (cyan dash line). Hence, our saturated design will be more feasible in practice. In contrast to the saturation control approach in [30], where the semiellipsoidal invariant set is considered, our approach allows the controller to attain the saturation bound to meet the tracking requirement.

Example 4: In this example, we provide a heterogeneous hierarchical pattern-varying formation to show the

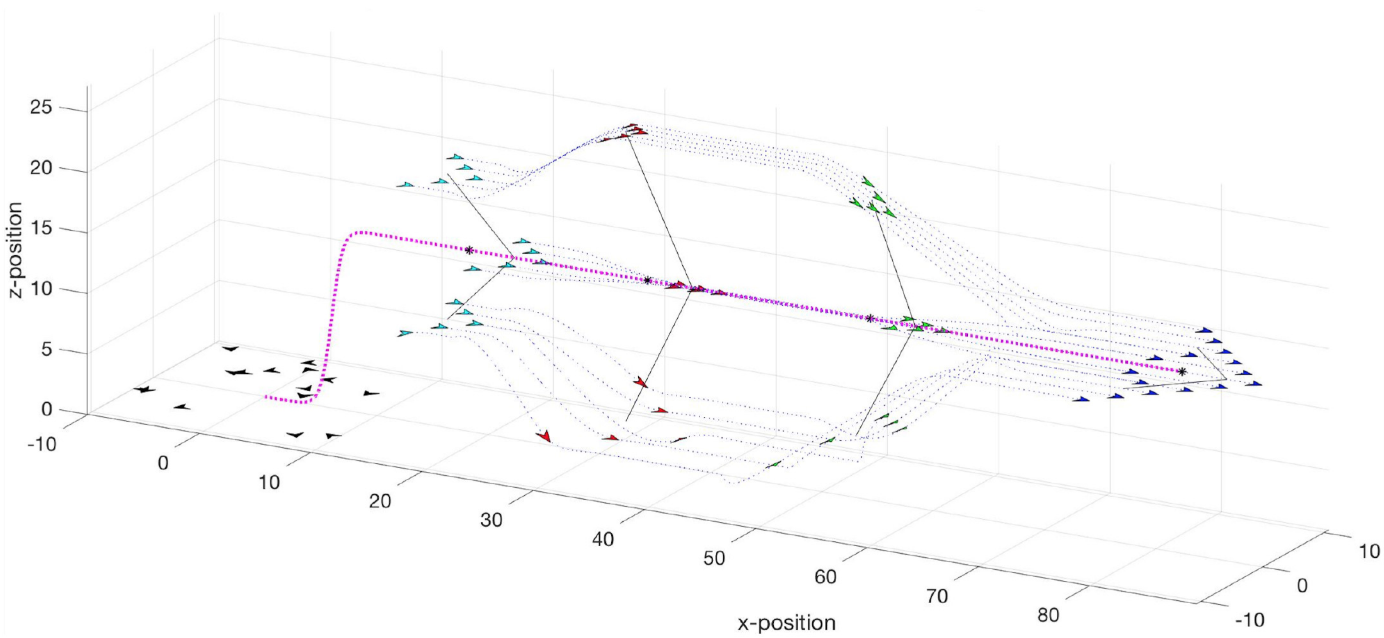

Fig. 10. Heterogeneous hierarchical structure of 3-D maneuver control, which shows the flexibility and variety of our design.

design flexibility of the proposed 3-D maneuver control. With the proposed relative descriptions, the strongly connected condition is the only requirement on communication. The simulation settings of Fig. 10 are as follows. The first hierarchy has three virtual agents, which serves as the references for second hierarchy. For each virtual agent, there are five agents to form its second hierarchy. The desired formation for the three virtual agents is the vertical check, while each second hierarchy forms the horizontal check, as shown with the black line and colored agents in Fig. 10, respectively. During execution, the desired formation of first hierarchy is stretched in z-direction, and is finally assigned to a 2-D plane. For each second hierarchy (subgroup), we can assign different transformations. As shown in the middle part of Fig. 10, the upper group is designed to shrink smaller and then restores to original size, while the bottom group is oppositely designed, that is, to enlarge and then restore. The middle group is to virtually shear into a line and then restore. The overall result is illustrated in Fig. 10, where the agents globally follow the first hierarchy and meanwhile, locally adjust with different transformation commands. Unlike the studies focus on rigidity, for example, [16], [20], [22], and [50], though rigidity ensures adorable transformation properties, it imposes hard limitations on communications. As a comparison, the design we proposed can be easily extended to *hierarchical* structure as long as the strongly connection is assured. Moreover, with the concept of the two-phase scheme discussed in Remark 6, different groups can be distinctly and *locally* adjusted, which reflects the term *heterogeneous*. To summarize, Example 4 demonstrates the flexibility and variety of our proposed design in 3-D maneuver control, where we can easily have extensions to hierarchical structure and covers formation in 2-D and 3-D spaces. It also shows the ability of time-varying adjustment for each hierarchy and the capability of local adjustments.

VIII. Conclusion

In this article, we proposed a novel 3-D maneuver controller with input constraints for MAS. The designed controller offers much more varieties for the formation and maneuver control of MAS and allows different combinations of behaviors such as the hierarchical structure maneuver control, which provides flexibility for different tasks, including pattern-varying formation, switching communications, and locally adjustments. By our design, the heading direction of each agent in the system will align to the direction of the formation, which differs from most of the formation controllers in the literature that do not consider the heading directions. Furthermore, compared with existing results, there are relatively few works discuss formation maneuver control of nonlinear system in three dimension. Our proposed 3-D design not only considers the nonholonomic constraints but also designs the saturated control input in the specified bound. The future directions of this work include presenting more scenarios for the controller and the switching signals, considering collision avoidance between agents based on the proposed insight of two-phase scheme, and implementing the practical system.

References

[1] S. Zhao and D. Zelazo, "Translational and scaling formation maneuver control via a bearing-based approach," *IEEE Trans. Control Netw. Syst.*, vol. 4, no. 3, pp. 429–438, Sep. 2017.

[2] J. R. T. Lawton, R. W. Beard, and B. J. Young, "A decentralized approach to formation maneuvers," *IEEE Trans. Robot. Autom.*, vol. 19, no. 6, pp. 933–941, Dec. 2003.

[3] Y. Xu, S. Zhao, D. Luo, and Y. You, "Affine formation maneuver control of high-order multi-agent systems over directed networks," *Automatica*, vol. 118, Aug. 2020, Art. no. 109004.

[4] L. Wang, H. He, Z. Zeng, and M.-F. Ge, "Model-independent formation tracking of multiple Euler–Lagrange systems via bounded inputs," *IEEE Trans. Cybern.*, vol. 51, no. 5, pp. 2813–2823, May 2021.

[5] B. Wang, W. Chen, J. Wang, B. Zhang, and P. Shi, "Semiglobal tracking cooperative control for multiagent systems with input saturation: A multiple saturation levels framework," *IEEE Trans. Autom. Control*, vol. 66, no. 3, pp. 1215–1222, Mar. 2021.

[6] M.-L. Chiang, Y.-W. Chen, C.-S. Chen, and S. T. Tsai, "Distributed formation control of multiagent systems with specified order," *IEEE Trans. Syst., Man, Cybern., Syst.*, vol. 52, no. 1, pp. 301–310, Jan. 2022.

[7] L. B. Arranz, A. Seuret, and C. C. de Wit, "Elastic formation control based on affine transformations," in *Proc. Amer. Control Conf.*, Jun. 2011, pp. 3984–3989.

[8] R. Wang, X. Dong, Q. Li, and Z. Ren, "Distributed time-varying formation control for multiagent systems with directed topology using an adaptive output-feedback approach," *IEEE Trans. Ind. Informat.*, vol. 15, no. 8, pp. 4676–4685, Aug. 2019.

[9] K.-K. Oh and H.-S. Ahn, "Formation control and network localization via orientation alignment," *IEEE Trans. Autom. Control*, vol. 59, no. 2, pp. 540–545, Feb. 2014.

[10] G. Jing and L. Wang, "Multiagent flocking with angle-based formation shape control," *IEEE Trans. Autom. Control*, vol. 65, no. 2, pp. 817–823, Feb. 2020.

[11] H. J. Asl, T. Narikiyo, and M. Kawanishi, "Saturated input consensus algorithms for perturbed double-integrator systems without velocity measurements," *Syst. Control Lett.*, vol. 133, Nov. 2019, Art. no. 104528.

[12] T. Han and W. X. Zheng, "Bipartite output consensus for heterogeneous multi-agent systems via output regulation approach," *IEEE Trans. Circuits Syst. II, Exp. Briefs*, vol. 68, no. 1, pp. 281–285, Jan. 2021.

[13] X. Li, F. Liu, M. Buss, and S. Hirche, "Fully distributed consensus control for linear multiagent systems: A reduced-order adaptive feedback approach," *IEEE Trans. Control Netw. Syst.*, vol. 7, no. 2, pp. 967–976, Jun. 2020.

[14] T. H. A. van den Broek, N. van de Wouw, and H. Nijmeijer, "Formation control of unicycle mobile robots: A virtual structure approach," in *Proc. 48th IEEE Conf. Decis. Control (CDC) Held Jointly 28th Chin. Control Conf.*, 2009, pp. 8328–8333.

[15] Z. Sun, H. G. de Marina, G. S. Seyboth, B. D. O. Anderson, and C. Yu, "Circular formation control of multiple unicycle-type agents with non-identical constant speeds," *IEEE Trans. Control Syst. Technol.*, vol. 27, no. 1, pp. 192–205, Jan. 2019.

[16] X. Li, M. J. Er, G. Yang, and N. Wang, "Bearing-based formation manoeuvre control of nonholonomic multi-agent systems," *Int. J. Syst. Sci.*, vol. 50, no. 16, pp. 2993–3002, 2019.

[17] K.-K. Oh, M.-C. Park, and H.-S. Ahn, "A survey of multi-agent formation control," *Automatica*, vol. 53, pp. 424–440, Mar. 2015.

[18] W. Ren, "Multi-vehicle consensus with a time-varying reference state," *Syst. Control Lett.*, vol. 56, nos. 7–8, pp. 474–483, 2007.

[19] Z. Sun and B. D. O. Anderson, "Rigid formation control with prescribed orientation," in *Proc. IEEE Int. Symp. Intell. Control (ISIC)*, 2015, pp. 639–645.

[20] S. Zhao and D. Zelazo, "Localizability and distributed protocols for bearing-based network localization in arbitrary dimensions," *Automatica*, vol. 69, pp. 334–341, Jul. 2016.

[21] Z. Sun, S. Mou, B. D. O. Anderson, and A. S. Morse, "Rigid motions of 3-D undirected formations with mismatch between desired distances," *IEEE Trans. Autom. Control*, vol. 62, no. 8, pp. 4151–4158, Aug. 2017.

[22] X. Luo, X. Li, X. Li, and X. Guan, "Bearing-only formation control of multi-agent systems in local reference frames," *Int. J. Control*, vol. 94, no. 5, pp. 1261–1272, 2021.

[23] J. Fu, G. Wen, X. Yu, and Z.-G. Wu, "Distributed formation navigation of constrained second-order multiagent systems with collision avoidance and connectivity maintenance," *IEEE Trans. Cybern.*, vol. 52, no. 4, pp. 2149–2162, Apr. 2022.

[24] X. Wang, Z. Zeng, and Y. Cong, "Multi-agent distributed coordination control: Developments and directions via graph viewpoint," *Neurocomputing*, vol. 199, pp. 204–218, Jul. 2016.

[25] Z. Lin, L. Wang, Z. Han, and M. Fu, "Distributed formation control of multi-agent systems using complex Laplacian," *IEEE Trans. Autom. Control*, vol. 59, no. 7, pp. 1765–1777, Jul. 2014.

[26] Y. Lv, J. Fu, G. Wen, T. Huang, and X. Yu, "On consensus of multiagent systems with input saturation: Fully distributed adaptive antiwindup protocol design approach," *IEEE Trans. Control Netw. Syst.*, vol. 7, no. 3, pp. 1127–1139, Sep. 2020.

[27] X. Dong and G. Hu, "Time-varying formation control for general linear multi-agent systems with switching directed topologies," *Automatica*, vol. 73, pp. 47–55, Nov. 2016.

[28] S. Tong, X. Min, and Y. Li, "Observer-based adaptive fuzzy tracking control for strict-feedback nonlinear systems with unknown control gain functions," *IEEE Trans. Cybern.*, vol. 50, no. 9, pp. 3903–3913, Sep. 2020.

[29] Y. Li, T. Yang, and S. Tong, "Adaptive neural networks finite-time optimal control for a class of nonlinear systems," *IEEE Trans. Neural Netw. Learn. Syst.*, vol. 31, no. 11, pp. 4451–4460, Nov. 2020.

[30] J. Lian and F. Wu, "Stabilization of switched linear systems subject to actuator saturation via invariant semiellipsoids," *IEEE Trans. Autom. Control*, vol. 65, no. 10, pp. 4332–4339, Oct. 2020.

[31] X. Wang, H. Su, M. Z. Q. Chen, and X. Wang, "Observer-based robust coordinated control of multiagent systems with input saturation," *IEEE Trans. Neural Netw. Learn. Syst.*, vol. 29, no. 5, pp. 1933–1946, May 2018.

[32] J. Fu, Y. Lv, G. Wen, X. Yu, and T. Huang, "Velocity and input constrained coordination of second-order multi-agent systems with relative output information," *IEEE Trans. Netw. Sci. Eng.*, vol. 7, no. 3, pp. 1925–1938, Jul.–Sep. 2020.

[33] J. Fu, Y. Wan, G. Wen, and T. Huang, "Distributed robust global containment control of second-order multiagent systems with input saturation," *IEEE Trans. Control Netw. Syst.*, vol. 6, no. 4, pp. 1426–1437, Dec. 2019.

[34] M. Long, H. Su, and Z. Zeng, "Output-feedback global consensus of discrete-time multiagent systems subject to input saturation via Q-learning method," *IEEE Trans. Cybern.*, vol. 52, no. 3, pp. 1661–1670, Mar. 2022.

[35] S. Hernandez and D. A. Paley, "Three-dimensional motion coordination in a spatiotemporal flowfield," *IEEE Trans. Autom. Control*, vol. 55, no. 12, pp. 2805–2810, Dec. 2010.

[36] W. Li and M. W. Spong, "Unified cooperative control of multiple agents on a sphere for different spherical patterns," *IEEE Trans. Autom. Control*, vol. 59, no. 5, pp. 1283–1289, May 2014.

[37] M. I. El-Hawwary, "Three-dimensional circular formations via set stabilization," *Automatica*, vol. 54, pp. 374–381, Apr. 2015.

[38] X. Luo, X. Li, X. Li, J. Yan, and X. Guan, "Globally stable formation control of nonholonomic multiagent systems with bearing-only measurement," *IEEE Syst. J.*, vol. 14, no. 2, pp. 2901–2912, Jun. 2020.

[39] L. Briñón-Arranz, A. Seuret, and C. Canudas-de-Wit, "Cooperative control design for time-varying formations of multi-agent systems," *IEEE Trans. Autom. Control*, vol. 59, no. 8, pp. 2283–2288, Aug. 2014.

[40] W. Ren, "Second-order consensus algorithm with extensions to switching topologies and reference models," in *Proc. Amer. Control Conf.*, Jul. 2007, pp. 1431–1436.

[41] Y.-W. Chen, M.-L. Chiang, and L.-C. Fu, "Formation control with orientation alignment and constrained input," in *Proc. 21st IFAC World Congr.*, 2020, pp. 3397–3402.

[42] E. D. Sontag, "Remarks on stabilization and input-to-state stability," in *Proc. 28th IEEE Conf. Decis. Control*, vol. 2, Dec. 1989, pp. 1376–1378.

[43] X. Zhao, L. Zhang, P. Shi, and M. Liu, "Stability and stabilization of switched linear systems with mode-dependent average dwell time," *IEEE Trans. Autom. Control*, vol. 57, no. 7, pp. 1809–1815, Jul. 2012.

[44] X. Yang, X. Li, J. Lu, and Z. Cheng, "Synchronization of time-delayed complex networks with switching topology via hybrid actuator fault and impulsive effects control," *IEEE Trans. Cybern.*, vol. 50, no. 9, pp. 4043–4052, Sep. 2020.

[45] X. Yang, Y. Liu, J. Cao, and L. Rutkowski, "Synchronization of coupled time-delay neural networks with mode-dependent average dwell time switching," *IEEE Trans. Neural Netw. Learn. Syst.*, vol. 31, no. 12, pp. 5483–5496, Dec. 2020.

[46] X. Yang, X. Wan, C. Zunshui, J. Cao, Y. Liu, and L. Rutkowski, "Synchronization of switched discrete-time neural networks via quantized output control with actuator fault," *IEEE Trans. Neural Netw. Learn. Syst.*, vol. 32, no. 9, pp. 4191–4201, Sep. 2021.

[47] D. Wang, D. Wang, and W. Wang, "Necessary and sufficient conditions for containment control of multi-agent systems with time delay," *Automatica*, vol. 103, pp. 418–423, May 2019.

[48] Q. Ma and S. Xu, "Consensus switching of second-order multiagent systems with time delay," *IEEE Trans. Cybern.*, early access, Aug. 11, 2021, doi: 10.1109/TCYB.2020.3011448.

[49] J. Zhang, M. Lyu, T. Shen, L. Liu, and Y. Bo, "Sliding mode control for a class of nonlinear multi-agent system with time delay and uncertainties," *IEEE Trans. Ind. Electron.*, vol. 65, no. 1, pp. 865–875, Jan. 2018.

[50] S. Zhao, D. V. Dimarogonas, Z. Sun, and D. Bauso, "A general approach to coordination control of mobile agents with motion constraints," *IEEE Trans. Autom. Control*, vol. 63, no. 5, pp. 1509–1516, May 2018.

Yu-Wen Chen received the B.S. and M.S. degrees in electrical engineering from National Taiwan University, Taipei, Taiwan, in 2016 and 2019, respectively. He is currently pursuing the Ph.D. degree with the Department of Electrical Engineering and Computer Science, University of California at Berkeley, Berkeley, CA, USA.

His current research interests include localization and formation control of robotic systems, motion planning of manipulators, and hierarchical guidance control.

Ming-Li Chiang (Member, IEEE) received the Ph.D. degree from the Department of Electrical Engineering, National Taiwan University, Taipei, Taiwan, in 2010.

From 2014 to 2016, he was a Visiting Scholar with the Department of Computer, Control, and Management Engineering, University of Rome La Sapienza, Rome, Italy. From 2017 to 2018, he was a Postdoctoral Researcher with National Taiwan University. Since 2020, he has been serving as an Assistant Professor with the Department of Applied Mathematics, Tunghai University, Taichung, Taiwan. His research interests include switched systems, nonlinear and adaptive control, system theory, multiagent system with unmanned vehicles, and applications of control engineering.

Dr. Chiang received the Best Paper Award in Chinese Automatic Control Conference in 2012.

Li-Chen Fu (Fellow, IEEE) received the B.S. degree from National Taiwan University, Taipei, Taiwan, in 1981, and the M.S. and Ph.D. degrees from the University of California at Berkeley, Berkeley, CA, USA, in 1985 and 1987, respectively.

Since 1987, he has been with National Taiwan University, and has been awarded an Irving T. Ho Chair Professor and an NTU Chair Professor since 2007 and 2020, respectively. He currently serves as the Director of NTU Center for Artificial Intelligence (AI) and Advanced Robotics as well as the Co-Director of Ministry of Science and Technology/NTU Joint Research Center for AI Technology and All Vista Healthcare. His research interests include social robotics, smart home, visual detection and tracking, virtual reality, and control theory and applications.

Dr. Fu has received numerous academic recognitions, such as the Distinguished Research Awards from National Science Council, Taiwan, the Macronix Chair Professorship, the Academic Award, as well as the National Chair Professorship from the Ministry of Education, Taiwan. He is currently serving as the Editor-in-Chief for the *Asian Journal of Control* as well as an Advisory Committee Member of Asian Control Association, and has served as the Vice-President of IEEE Control Systems Society from 2017 to 2018. He was an IFAC Fellow in 2017.